Magnetic Field Positioning Technology of Indoor Sports Bodies

Kai Li, *Member, IEEE*, Qingqing Gong, Yajun Ren, Yuan Li, Yan Han, Cunsuo Pang, and Huihua Kong

***Abstract*—Aiming at the problem of the failure of the global positioning system in the satellite denied environment, and facing the needs of the navigation and positioning in indoor space, the technology of indoor magnetic field vector positioning and navigation have been studied. Based on the geomagnetic matching technology, the wavelet analysis method is used to estimate the noise components and statistical characteristics of the magnetic field three-dimensional signal; combined with the Kalman filtering algorithm, through estimating and optimizing the magnetic field vector signal, an indoor magnetic positioning signal processing algorithm with wavelet analysis and Kalman fusion is established, realizing the optimization of the measurement accuracy of the geomagnetic signal and the accuracy of the fingerprint map. The experimental results indicate that the signal-to-noise ratio of the test sequence is increased by 3db, the root mean square error is reduced by about 30%, and the maximum positioning error reaches 1.34m, which can meet the requirements of indoor positioning.**

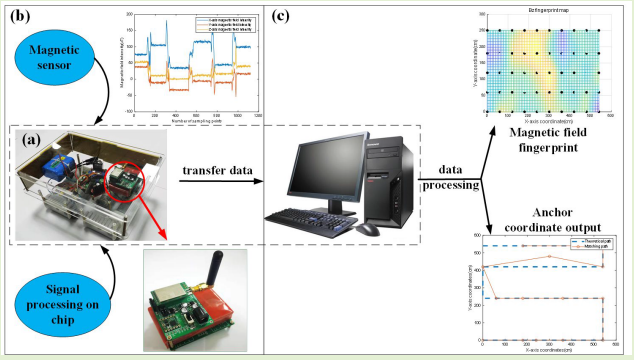

***Index Terms*—Geomagnetic filtering algorithm, indoor navigation, Kalman filtering, satellite denial, wavelet analysis.**

I. Introduction

SINCE people spend most of their time in an indoor environment in daily life, location-based services (LBS) play a more important role in the scenario such as security rescue operations, navigation in buildings, and big data analysis [1]. Indoor location service is applied in large indoor scenes such as large warehouses, factories, airports and convention centers. Under complex indoor environment conditions, indoor location technology can effectively provide personnel location information. Indoor positioning can provide indoor navigation and personnel positioning services for operators, and can be used for protection management of hospital isolation area, patrol inspection of large equipment in the factory, personnel control in office area, personnel location determination of rescue operations, etc. However, when used in an indoor environment, Global Positioning System (GPS) service may fail to provide LBS due to too long signal propagation and too much signal attenuation of the satellite to penetrate the buildings [2]. Therefore, it is necessary to research other methods to provide indoor positioning services in GPS denied environment. Researchers have used the technologies such as pedestrian dead reckoning (PDR), camera image recognition [3], ultrasonic positioning [4], Wifi positioning [5], ultra-wideband (UWB) [6], infrared [7], radio frequency identification (RFID) [8], LED visible light [9], ZigBee [10], Bluetooth [11], and geomagnetism [12] to build up indoor positioning systems, which are mounted on the devices such as robots [13] and drones [14] for indoor positioning scenarios such as indoor vehicles and personnel navigation. Among the above indoor positioning technologies, the positioning technologies based on WiFi received signal strength indication (RASS) [15], Bluetooth, smartphone, lighting, etc. rely on the infrastructure in the building, with high positioning accuracy, and the positioning effect are greatly affected by the visibility and positioning distance in the environment [16]. Using ultrasonic, UWB [17], infrared light, RF, ZigBee and other technologies need to set up additional signal transmitting devices in the positioning area, while PDR system, image recognition and positioning technology based on camera and geomagnetic positioning technology do not depend on the

Manuscript received October 21, 2021; revised November 17, 2021; accepted November 17, 2021. Date of publication November 18, 2021; date of current version December 29, 2021. This work was supported in part by the Natural Science Foundation of Shanxi Province, China, under Grant 201903D121133 and Grant 201901D211251. The associate editor coordinating the review of this article and approving it for publication was Prof. Guiyun Tian. *(Corresponding author: Kai Li.)*

Kai Li, Qingqing Gong, Yajun Ren, Yan Han, Cunsuo Pang, and Huihua Kong are with the Key Laboratory of Information Detection and Processing in Shanxi Province, North University of China, Taiyuan 030051, China (e-mail: likai@nuc.edu.cn; s1905076@st.nuc.edu.cn; s19005036@st.nuc.edu.cn; hanyan@nuc.edu.cn; pangcunsuo@126.com; huihuak@163.com).

Yuan Li is with the College of Information and Communication Engineering in Shanxi Province, North University of China, Taiyuan 030051, China (e-mail: liyuan82@nuc.edu.cn).

Digital Object Identifier 10.1109/JSEN.2021.3129330

infrastructure and additional signal transmitting devices in the building. Only the signal acquisition device is needed to collect indoor information, and the effect is hardly affected by the presence of obstructions. The indoor environment area is small, the magnetic field change in small area is small, the magnetic field distribution is relatively uniform, and the difference of magnetic field intensity is small; However, there are many magnetic fingerprint data in large outdoor areas, the magnetic field distribution is uneven, and the magnetic field intensity varies greatly. Therefore, the fingerprint location method based on parameters such as magnetic field vector is suitable for providing location services in small indoor areas.

The positioning technology relying on indoor infrastructure is often limited by the working conditions of infrastructure, and the geomagnetic field exists at any time. Therefore, indoor positioning through geomagnetic field characteristics is more stable.Theoretically, the geomagnetic field feature information at any point in the near-Earth space is unique. Taking the geomagnetic field data characteristics at each point in the geographic location as the basis for indoor positioning, the magnetic field positioning technology matches the data collected by the magnetic sensor with the magnetic fingerprints in the geomagnetic fingerprint to provide LBS [18]. The characteristic parameters of the geomagnetic field can be the total magnetic field vector or the components in three directions decomposed from the total magnetic field vector according to a three-dimensional coordinate system with three axes perpendicular to each other [19]. Since the magnetic field intensity of the geomagnetic field is weak and the spectrum range is wider, the magnetoresistive sensor is very susceptible to interference from the carrier or other magnetic fields when detecting the geomagnetic field [20]. As the collected information contains a variety of noises and there exist many points with similar magnetic field parameter values on the single-axis geomagnetic fingerprint, these two magnetic signal characteristics tend to affect the accuracy of geomagnetic positioning, and the filtering processing of the collected magnetic field information is conducive to improving the accuracy of geomagnetic matching. In order to reduce the interference of noise on the positioning accuracy, researchers have proposed different solutions. Xiaokang Qi et al, used the Kalman filter algorithm to match the magnetic field spatial angle of the positioning point to the magnetic gradient map, achieving the positioning function, improving the positioning accuracy of the road sign system to cm [21]; Yuanchao Shu et al, used the positioning method of the ground magnetic field signal and the WiFi signal fusion, and the initial position of the magnetic field matching was limited by the WiFi positioning, and the percentage of error of the results less than 1m was increased [22]; Kok-Meng Lee et al, applied the improved Dynamic Time Warping (DTW) methods to one-dimensional magnetic map matching. By estimating the optimal route, the total amount of matching sequence was significantly reduced, and the corner path point error in the experiment prediction was approximately 0.15m [23]; Binhee Kim et al, proposed to use a Bayesian filtering algorithm based on the measured difference (MD) likelihood function to predict the position, the experimental results indicate that this algorithm had reduced the complexity of the algorithm matching process [24]; Bimal Bhattarai et al, used a three-layer deep recurrent neural network (DRNN) model to classify the landmarks corresponding to the magnetic field data, and the experimental effect was better than that of the traditional shallow neural network structures such as KNN, SVM, logistic, etc [25]. Professor Lingfeng Shi's team proposed the technology of eliminating fingerprint time accumulation error using general sensory calibration source (GSCS) and relevant measurement indicators, and applied it to the indoor magnetic map positioning method of inertial sensor and magnetic sensor fusion [26]; the team also proposed a geomagnetic and accelerometer indoor positioning matching algorithm integrating particle filter and pedestrian dead reckoning (PDR), which uses gait detection error to limit the area of particle generation [27], reducing the computational complexity of particle magnetic fingerprint matching. Professor Xiaoji Niu's team used the extended Kalman filtering method to estimate the mileage scale and wheel angle error of the navigation robot, constrained the time cumulative error of the inertial navigation system, and improved the accuracy of yaw angle measurement in the navigation process [28]. Alwin Poole team designed a Kalman filtering algorithm integrating accelerometer, gyroscope and magnetometer data. Compared with using a single sensor, the average heading error is as small as 4.72° [29]. Grottke, Jan's team combines inertial navigation unit and fingerprint based positioning unit, provides indoor positioning service based on smart phone with the help of sensors, wireless LAN, Bluetooth and other devices, and uses Bayesian filtering method to weight the position estimated by multiple sensors [30].

At present, the filtering algorithms related to geomagnetic positioning mainly include particle filtering (PF), Bayesian filtering, Kalman filtering (KF), etc, of which the particle filters are mostly used to process geomagnetic data, and the filtering convergence effect is affected by the indoor geomagnetic distribution, and the sampling according to the probability distribution is prone to the circumstance of filtering divergence, which will eventually lead to larger positioning errors [31]; Bayesian filtering cannot obtain analytical solutions in most cases without limiting conditions. Kalman filtering as the further derivation of Bayesian filtering for system state values conforming to Gaussian distribution can obtain the analytical signal when filtered off in the case of known noise statistics.

Compared with single system positioning, many combined systems have better positioning accuracy. For example, the average positioning error of common fusion PDR and WiFi systems is about 1.5m-2m, which is better than WiFi fingerprint and trilateral measurement methods [32]. Multiple combined systems often weight the results of multiple positioning technologies, which reduces the error of the overall system and obtains more accurate positioning results. Reducing the positioning error of a single system is helpful to improve the positioning accuracy of the combined system. Specific to the problem that the statistical characteristics of noise are unknown in the process of magnetic field positioning, a geomagnetic positioning method with the fusion of wavelet analysis and Kalman filtering is proposed in this paper, which utilizes the wavelet analysis method to estimate the multi-

source noise components and statistical characteristics in the three-dimensional magnetic field signal, filters and optimizes the single-point magnetic field signal, and matches the signal with the magnetic field fingerprint map to realize the positioning function, combined with the Kalman filtering algorithm. Under the precondition that the geomagnetic signal is assumed to satisfy the Gaussian distribution, the denoising effectiveness of the wavelet-Kalman fusion filtering method and the wavelet analysis method on noisy signals is simulated and compared in this paper, verifying the feasibility of this filtering algorithm; 100 reference points within a 5.4m*5.4m indoor area are acquired to plot the geomagnetic fingerprints, the position coordinates of the 16 segments of stationary sequences in the test sequence are matched and located, and the error range of the positioning points is calculated.

The rest of the paper is organized as follows——Section 2 introduces the relevant principle knowledge of indoor positioning using magnetic signal. Section 3 introduces the related algorithms of fingerprint matching and magnetic signal processing using magnetic signal. Section 4 gives the experimental device and result analysis. Finally, section 5 summarizes the work of this paper and gives the future development direction.

II. Related Knowledge

This section will briefly introduce the relevant principles of magnetic field positioning, including geomagnetic positioning principle, magnetic signal processing and estimation algorithm.

A. Geomagnetic Positioning

The geomagnetic field is one of the natural features of the earth, expressed as the size (approximately the total intensity is about $23-66\mu T$), direction, and spatial distribution, and the geomagnetic data characteristics at each point in the geographic location are unique [33]. When collecting the three-axis magnetic field intensity on the same location at different moments within one day for about 1 minute of magnetic field data at each moment, the average value is calculated and plotted to obtain Table I, from which it can be known that the three-axis magnetic field intensity at different moments at the same point changes little, with the maximum difference of the uniaxial magnetic field intensity less than 10μT, so the intensity of the geomagnetic field can be used as a basis for positioning. When comparing the collected three-axis magnetic field data with the off-line three-axis geomagnetic field fingerprints, the location to be positioned $\{x, y\}$ can be determined.

The indoor positioning based on the geomagnetic field is essentially the geomagnetic field matching, which is usually achieved by calculating the correlation degrees between the three-axis magnetic data of the point to be located and the geomagnetic field fingerprint with the process as shown in the figure: each magnetic fingerprint includes two-dimensional position coordinates and triaxial magnetic field component information, a large number of three-axis geomagnetic field data is collected in advance to plot 3 geomagnetic fingerprint maps, as shown in Fig. 1 (a), including the coordinates of each point and three-axis magnetic field intensity, compared with the single axis magnetic field information, the matching accuracy of fingerprint is higher. The prerequisite for drawing geomagnetic fingerprint maps is to collect a large number of geomagnetic field intensity data in the experimental area, but the collected reference points corresponding to the area of the experimental area is relatively small, for which a two-dimensional interpolation method can be used to expand the points and corresponding data in the reference map, which is helpful to establish an indoor geomagnetic field map, including Kriging interpolation method, weighted interpolation method [34], neighbor interpolation method, etc. and the nonlinear Gaussian process regression method, etc. Then, the magnetic field information at the point where the object is located, as shown in Fig. 1 (b) is matched with the magnetic field information at each point in the corresponding single-axis geomagnetic fingerprint map to perform fingerprint recognition on the basis of the existing geomagnetic field fingerprint map to finally identify the current position where the object locates. Magnetoresistive sensors can collect magnetic field intensity components in three directions perpendicular to each other. Different magnetoresistive sensors may collect different readings for the same magnetic field; as can be seen from Fig. 1 (c), the magnetic field component data collected by the sensor contains noise information, that is, the curve segments parallel to the time axis in the figure contain glitch fluctuations in different sizes. It can be known from physics that the geomagnetic field data will be interfered by different sources. For example, electromagnetic interference sources such as indoor computers, mobile phones, machinery equipment will interfere with the intensity of the geomagnetic field. Therefore, it is necessary to perform the filtering smooth processing on the raw data collected by the sensor, so as to get the images with better effect, for which the common filtering methods include wavelet threshold denoising, FIR filtering, Butterworth filtering, moving average filtering, median filtering, and so on. The filtering algorithm is studied in this paper specific to the collected data by a single-type magnetoresistive sensor and an MPU9250 sensor is selected to collect the geomagnetic field data, during which one point is measured multiple times to reduce the influence of equipment noise and measurement errors, and a filtering algorithm is used during the data processing session to further reduce noise, and compare the processed magnetic field data with the data in the geomagnetic fingerprint map, which is beneficial to improve the matching accuracy of geomagnetic positioning.

TABLE I
SCHEMATIC DIAGRAM OF THE MAGNETIC FIELD INTENSITY AT DIFFERENT MOMENTS AT A FIXED POINT

Moment	X-axis magnetic field intensity/ μ T	Y-axis magnetic field intensity/ μ T	Z-axis magnetic field intensity/ μ T
8:50	66.4833	-34.7708	0.5093
9:59	63.7563	-32.8969	-1.0484
10:55	66.1684	-35.1017	0.4036
11:28	66.1467	-34.0506	-1.3474
15:56	67.3955	-34.9174	-0.1585
16:58	64.5816	-33.5816	-0.4150

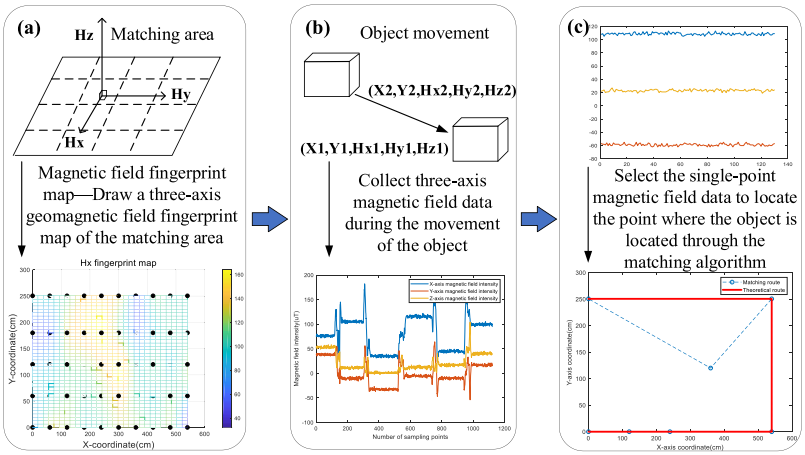

Fig. 1. Diagram of geomagnetic positioning process.

B. Kalman Filtering

In the process of positioning using magnetic field information, the data collected by magnetic sensor contains noise, and the distribution model of noise is similar to Gaussian distribution [35], and Kalman filter is suitable for processing the signal whose noise statistical characteristics comply with Gaussian noise. Therefore, the positioning technology proposed in this paper uses Kalman filter method to process the data collected by sensor. Kalman filtering method estimates the state value of the next time based on the system state and linear function of the previous time. For the static magnetic field information acquisition process, the state transition of the previous time and the next time conforms to the linear equation, and the state values of the previous and later times are the same constant value.

As for a certain dynamic system, formula (1) can be used to describe the relationship between the state quantity and the observed quantity.

$$\begin{cases} X(k) = \Phi X(k-1) + \Gamma W(k-1) \\ Y(k) = H X(k) + V(k) \end{cases} \tag{1}$$

In the formula, k represents the moment of discrete, $X(k)$ is the state value of the system at moment k, which can be represented by the state value $X(k-1)$ at the previous moment and the input noise $W(k-1)$ in the system between the two moments, Φ is the state transition matrix, and Γ is the noise drive matrix that reflects the change of the input noise; H is the measurement matrix, which reflects the connection between the state quantity and the observed quantity in the system, and $V(k)$ is the noise introduced during the observation process.

When using Kalman filtering algorithm to process single variable data, the basic formula is as shown in formula (2):

$$\begin{cases} P(k+1|k) = \Phi P(k|k)\Phi^T + \Gamma Q \Gamma^T \\ \hat{X}(k+1|k) = \Phi \hat{X}(k|k) \\ \varepsilon(k+1) = Y(k+1) - H\hat{X}(k+1|k) \\ K(k+1) = P(k+1|k)H^T[HP(k+1|k)H^T + R]^{-1} \\ \hat{X}(k+1|k+1) = \hat{X}(k+1|k) + K(k+1)\varepsilon(k+1) \\ P(k+1|k+1) = [I_n - K(k+1)H]P(k+1|k) \end{cases} \tag{2}$$

The process of Kalman filtering is as follows: In the first step, it is necessary to estimate the variance matrix $P(k+1\,|k)$ at the next moment based on the variance matrix $P(k\,|k)$ at the previous moment, and to estimate the new state value $\hat{X}(k+1\,|k)$ based on the state value and the state transition matrix at the previous moment; the second step, calculate the error $\varepsilon(k+1)$ between the estimated value and the observed value and the Kalman gain $K(k+1)$; the third step is to use the error value and the Kalman gain to predict and update the previous state estimation value to obtain the final filtering result $\hat{X}(k+1\,|k+1)$.

This section only introduces the basic general formula of Kalman filter. When Kalman algorithm is used to process magnetic signals, the state equation and observation equation of the system where the magnetic sensor is located can be determined to effectively use Kalman algorithm to process the magnetic field signals collected in the positioning system. Therefore, the five matrices in the equation are very important. The details of determining the correlation coefficients of the two equations in the Kalman algorithm will be described in Section B of part III.

III. Geomagnetic Signal Processing

After the sensor collects the magnetic field data, it enters the second stage of geomagnetic positioning. It is necessary to compare and match the data to be matched with the three-axis magnetic fingerprint to obtain the coordinates of the points to be located. The time range of the data segment to be matched is short, and the noise has a great impact on the magnetic field data. The original signal needs to be filtered and compared with the fingerprint after reducing the influence of noise, which can improve the positioning accuracy of matching.

A. Matching Algorithms for Magnetic Field Positioning

Commonly used geomagnetic matching algorithms include the Magnetic Contour Matching (MAGCOM) algorithm based on correlation analysis, the geomagnetic matching algorithm based on Iterative Closest Contour Point (ICCP), and the geomagnetic matching algorithm based on the artificial fish swarm [36], of which the matching algorithms based on

correlation analysis mainly focus on the similarity degree, difference degree, and Hausdorff distance of the data any reference point in the measurement data and fingerprint map. The algorithms matched based on the similarity degree of the two include cross-correlation (COR) algorithm, correlation coefficient (CC) algorithm, product correlation (PROD) algorithm, and normalized product correlation algorithm (NPROD); the algorithms matched according to the disparity degree between the two include mean absolute difference (MAD) algorithm, mean square error (MSD) algorithm, absolute difference (AD) algorithm, square difference (SD), and sum of absolute differences (SAD) algorithm [37]. The SAD algorithm is selected in this paper for magnetic field data matching. This algorithm is often used in image matching algorithms with the basic process as: selecting a certain sequence from the test data, and then dividing the fingerprint into several image collections of the same size as the sequences, and calculating the difference between the corresponding elements in the sequences, summing up, and finally selecting the sequence with the minimal sum of errors as the matching sequence. The correlation index function of the SAD algorithm is as shown in formula (3):

$$C_i = \sum_{s=1}^{M}\sum_{t=1}^{N} |H_i(s,t) - A(s,t)| \tag{3}$$

In the formula, M and N are the number of rows and columns of the image to be matched, and C_i is the absolute differences between the i-th sub-image in the reference image and each point of the sequence to be matched. For the matching of single-point magnetic field intensity, this paper chooses to compare the processed magnetic field components with the fingerprint maps of the three-axis geomagnetic field components respectively, that is, as shown in equation (4):

$$D_i = |H_X(i) - H_x(A)| + \left|H_Y(i) - H_y(A)\right| + |H_Z(i) - H_z(A)| \tag{4}$$

In the formula, $H_X(i), H_Y(i), H_Z(i)$ represents the three-axis magnetic field intensity value of the i-th reference point in the magnetic fingerprint map, and $H_x(A), H_y(A), H_z(A)$ represents the three-axis magnetic field intensity data of Point A to be matched. The point with the minimal sum of absolute error between the measured point and the matched point is selected as the optimal matching point; when the matching points are finally connected and displayed, the positioning error can be obtained by comparing the theoretical routes with the matching process as shown in Fig. 2.

B. Data Processing Method Based on the Fusion of Wavelet and Kalman Filtering

The Kalman filtering algorithm is used to process the signal of three-axis magnetic field intensity collected by the magnetic sensor, which can reduce the noise in the magnetic field data. It is assumed that the system where the magnetic sensor is located conforms to the state equation and observation equation, as in formula (5):

$$\begin{cases} X(k) = X(k-1) + \Gamma W(k-1) \\ Y(k) = X(k) + V(k) \end{cases} \tag{5}$$

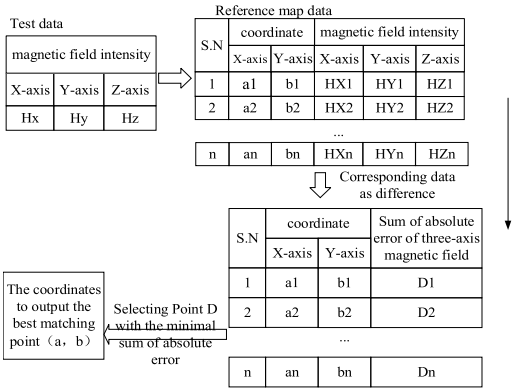

Fig. 2. Operation flow chart of SAD matching algorithm.

In the formula, $X = [x_1, \ldots, x_n]$ is the measured value, which is substituted into the geomagnetic field intensity components of the x-axis, y-axis, and z-axis, respectively, the data processed in this paper is the magnetic field strength data of a certain point in the static state. Theoretically, the state value at any time is the same value, that is, the magnetic field strength data at the previous time and the later time are the same, so the state transition matrix is 1. As process noise, the noise in the original signal can be filtered by wavelet analysis to obtain the statistical characteristics of process noise. $Y = [y_1, \ldots, y_n]$ is the data of the magnetic field component of each axis from Kalman filtering; the state quantity and the observed quantity are both the components of three-axis magnetic field, therefore, the observation matrix H is 1; $V = [v_1, \ldots, v_n]$ is the unknown system observation noise, the variance of observation noise is a statistical parameter. After long-term probability statistics on the data measured by the sensor, the measurement error of magnetic sensor and the variance of observation noise can be obtained, since the geomagnetic field intensity of the fixed point is filtered, the geomagnetic field intensity hardly changes, and the state transition matrix Φ in the state equation can be regarded as 1.

When using Kalman filter to process the three-axis magnetic field component data of a fixed point, the precondition is that the estimated value $\hat{X}(0)$ of the initial state, the initial variance $P(0)$, the process noise variance Q of the system and the observed noise variance R are known. $\hat{X}(0)$ is the estimate of the initial magnetic field state $X(0)$, which satisfies the formula $\hat{X}(0) = \mu_0$, and the value that is acquired is the average value of multiple sampling values; $P(0)$ is the variance of the initial magnetic field observed value, which satisfies the formula $P(0) = P_0$, and the value that is acquired is equal to the square of the difference value between the initial measurement value and the predicted initial observed value, that is

$$P(0) = \frac{1}{n}\sum_{j=1}^{n}(X_j - \frac{1}{n}\sum_{i=1}^{n}X_i)^2.$$

The observed noise variance is a statistical characteristic parameter of noise, reflecting the accuracy of the data collected by the magnetic sensor, which can be represented by the variance of the magnetic field intensity of a certain point continuously

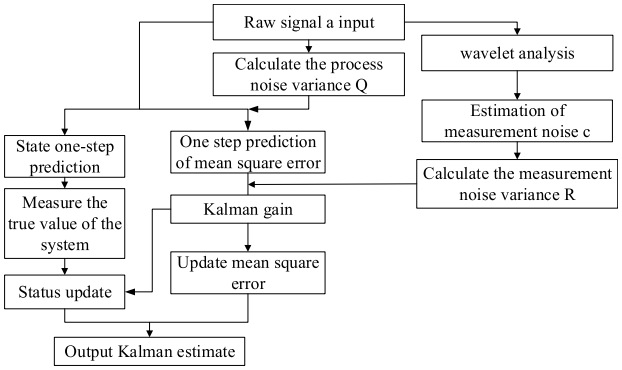

Fig. 3. Flow chart of wavelet and Kalman fusion filtering.

collected by the sensor; the process noise variance is the variance of other noise signals in the collection process.

The noise signal in the acquisition process is unknown. The wavelet analysis method is adopted in this paper to denoise the signal to be matched. By calculating the difference of signal A to be matched with signal B obtained after wavelet denoising, the estimated value C of the noise from the wavelet analysis on the process that the magnetic sensor collects the geomagnetic component information can be obtained, that is, the estimated value of noise is $C = A - B$. When calculating the noise variance according to the estimated noise C, fusing the Kalman filtering method, and re-performing the filtering processing of the signal to be matched, the filtering effect is better than that of the wavelet analysis method.

The flow chart of Kalman filtering algorithm combined with wavelet analysis algorithm is shown in Fig. 3. The main advantage of this filtering algorithm is to use wavelet analysis to estimate the system noise and white noise in the collected magnetic field data. The noise signal in the acquisition process is unknown, and the traditional Kalman filter is lack of necessary conditions. The wavelet analysis method can be used to reduce the noise of the processed signal. Through the subdivision of the original signal by wavelet in time and space frequency, part of the noise of the original signal is filtered, and the signal after wavelet denoising is obtained; Then, the original signal A is compared with the signal B obtained after wavelet denoising, and the estimated value C of noise in the process of collecting geomagnetic component information by wavelet analysis can be obtained, that is, the estimated value of noise filtered by wavelet analysis is $C = A - B$. The variance R of the observation noise $V(k)$ can be calculated according to the estimated noise C, and the variance Q of the process noise $W(k)$ can be estimated according to the variance of the data collected by the sensor for a long time. The Kalman filtering method is fused to filter the signal to be processed again. The process of Kalman filtering is as follows: in the first step, the new state value $\hat{X}(k+1\,|k)$ is estimated according to the state value and state transition matrix of the previous time, and the variance matrix $P(k+1\,|k)$ of the next time needs to be estimated according to the variance matrix $P(k\,|k)$ of the previous time; The second step is to calculate the error $\varepsilon(k+1)$ and Kalman gain $K(k+1)$ between the estimated value and the observed value; In the third step, the

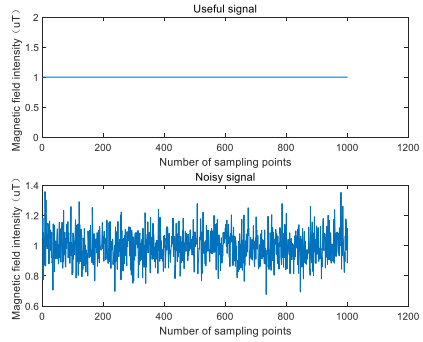

(a)Analog acquisition signal

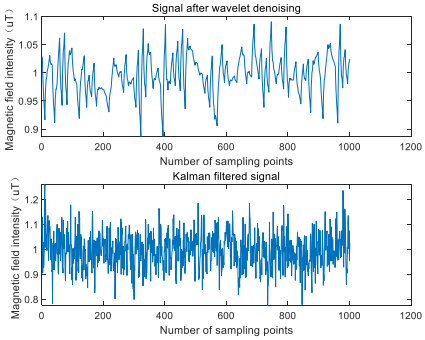

(b) Comparison chart of wavelet denoising and Kalman filtering

Fig. 4. Schematic diagram of analog filtering.

error value and Kalman gain are used to predict and update the previous state estimation value to obtain the final filtering result $\hat{X}(k+1\,|k+1)$.

The signal with constant function plus noise is used to verify the above filtering algorithm, where the constant function signal is $I = 1$, Gaussian white noise with SNR $10dB$ is added, and the constant function signal and the noisy signal are shown in Fig. 4 (a), their noise energy is smaller than that of useful signal. Formula $SNR = 10\log\frac{Ps}{Pn}$ is used to calculate the SNR, of which Ps is the signal energy and Pn is the noise energy, and the SNR is $19.9187dB$, the formula for calculating the root mean square error of the observation signal is

$$RMSE = \sqrt{\frac{1}{n}\sum_{i=1}^{n}(In_i - Ih_i)^2},$$

where In is the observation signal, Ih is the real signal value, and the root mean square error (RMSE) of the original signal is 0.0980; at this moment, for which the wavelet analysis method is sued to denoise the noisy signal, and the obtained signal is shown in Fig. 4 (b), and the SNR is $29.6622dB$ at this moment; the statistical characteristics of the noise estimator are obtained through wavelet denoising, and the calculated noise variance is substituted into the Kalman filtering process and the filtered signal obtained by Kalman filtering on the analog acquisition signal is shown in Fig. 4 (b), the SNR is $23.2309dB$ and RMSE is 0.0684 at this moment, resulting in that the signal waveform after Kalman filtering is smoother than the unfiltered signal waveform with fewer spikes, the signal-to-noise ratio is reduced by about and the mean square

Fig. 5. Schematic diagram of analog filtering.

error is reduced by about 0.0296. These two indexes for evaluating the filtering results show that the deviation between the Kalman estimated value and the real value is smaller than that between the noisy signal and the real value, from which it can be seen that this filtering method can effectively filter off the noise in the test sequence signal and improve the SNR.

IV. Experiment on Geomagnetic Positioning

In order to verify the magnetic field positioning technology proposed in this paper, we select some areas of the laboratory conference room as the experimental area, which is a small square area of 5.4m * 5.4m, in which 9 conference tables are placed.

A. Establishment of Geomagnetic Reference Map

The data collected by the magnetoresistive sensor includes the three-axis magnetic field intensity data of 100 reference points in the experimental area. The position distribution of 100 reference points is shown in Fig. 5. At present, the magnetic field fingerprint is two-dimensional, that is, the magnetic field distribution close to the ground height. The data collection time at each reference point in the experimental area is not less than 30s to reduce the error of the magnetic field component information of the magnetic field reference point caused by abnormal data values. Choosing a small area for indoor positioning experiment has the following advantages: 1. Uniform magnetic field distribution and obvious magnetic field characteristics; 2. The three-axis magnetic field strength parameters of each reference point have little difference, and the positioning error can be calculated better.

It is very important to plot a high-precision magnetic field component fingerprint map for magnetic field positioning. The more the number of magnetic field reference points is, the higher the positioning accuracy. Therefore, interpolation methods are needed to expand the data. Commonly used three-dimensional interpolation methods include Kriging interpolation, Scatteredinterpolant interpolation, etc. When comparing the interpolation results, Kriging interpolation method with a better interpolation effect is selected to interpolate the original 10*10 grid data to a 50*50 grid to make the fingerprint data more detailed to facilitate subsequent data matching. When obtaining the magnetic field intensity data

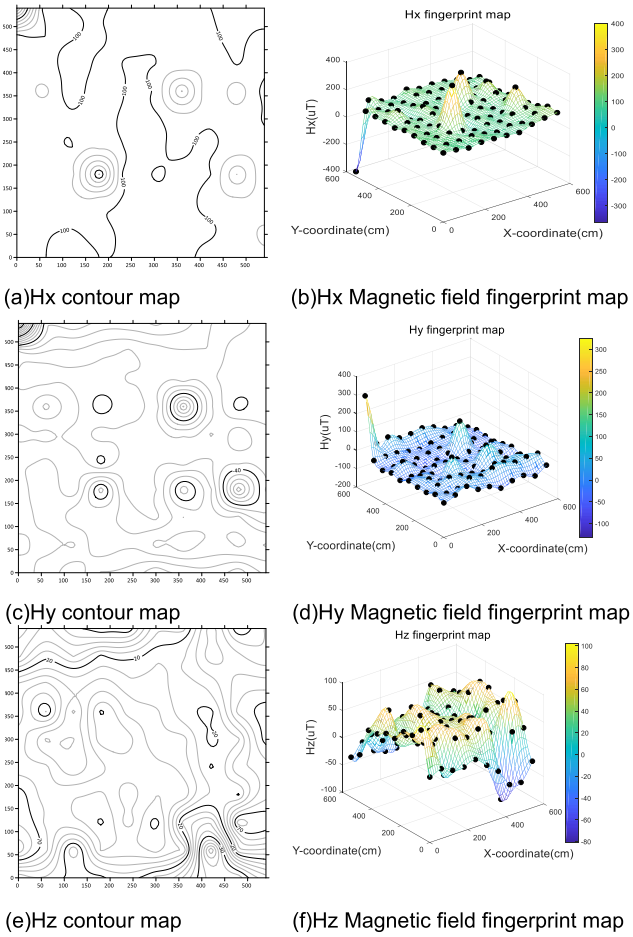

Fig. 6. Magnetic field distribution map of the positioning area.

of multiple magnetic reference points by averaging method, a kind of grid drawing software is employed to draw the contour map of the magnetic field components, as shown in Fig. 6 (a), (c), (e), and a kind of data analysis software is used to draw the fingerprint map for geomagnetic field component, and the magnetic field characteristic fingerprints are used to establish a fingerprint library for geomagnetic field components as shown in Fig. 6 (b), (d), (f), including the magnetic field component fingerprint maps of X-axis, Y-axis, and Z-axis, in which the black dots are the reference points where the actual data are collected, the grid intersection points are the reference points after interpolation, and the value of the involved magnetic field component data is taken as the mean value of multiple sampling measurements. In the subsequent positioning process, the magnetic field components collected from the stationary segments of each signal in the walking route are compared with the fingerprint maps of the geomagnetic field components to achieve positioning.

B. Kalman Filtering of Test Data

The error of magnetic sensor obeys Gaussian distribution, image display of the three-axis magnetic field data collected during the motion is performed, as shown in Fig. 7, from which it can be seen that a total of 16 segments of the sequences with relatively stable magnetic field intensity are

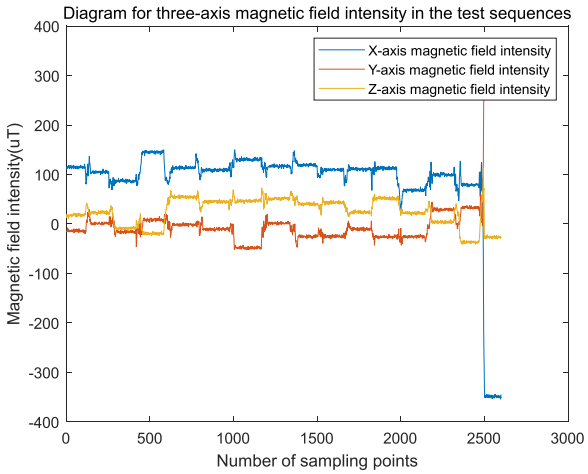

Fig. 7. Diagram for three-axis magnetic field intensity in the test sequences.

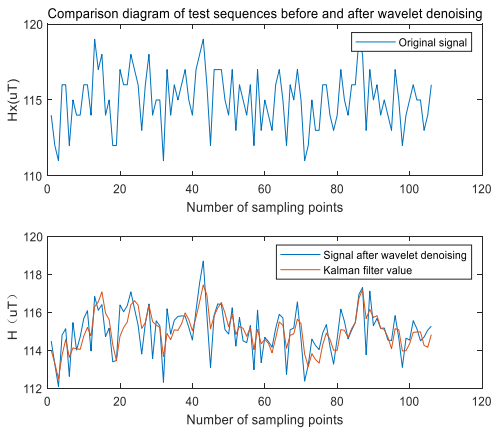

Fig. 8. Noise estimator extracted by wavelet denoising.

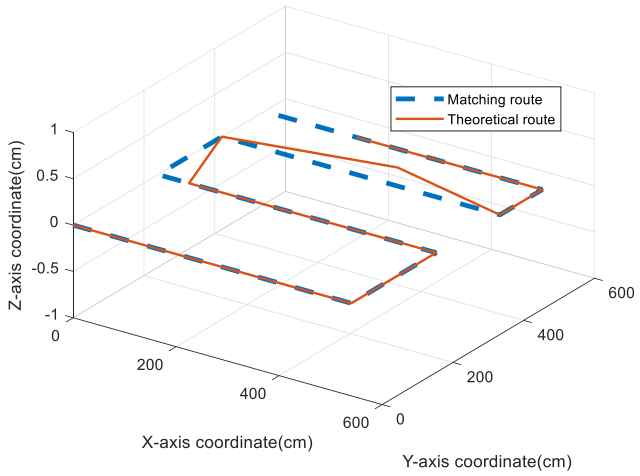

Fig. 9. Schematic diagram of matching path.

collected during the test process. These stationary sequences should be the magnetic field intensity data collected by the sensor at a certain fixed point when pausing for a longer time (about 10s). The coordinates of such a point can be estimated by matching the geomagnetic fingerprints on this stationary sequence. In this case, the sensor has successively passed these points, and when these points matched with these stationary sequences are connected in chronological order, it can roughly reflect the path that the sensor traverses in the test process.

Filtering experiment: Data processing is performed on the geomagnetic data at each segment of the stationary sequences, the magnetic field intensity component of the X-axis is first selected for wavelet analysis, where the wave with appropriate db is selected for multi-layer decomposition and denoising, to get the signal after wavelet denoising as shown in Fig. 8. By calculating the difference of the original signal with the signal after wavelet denoising, the noise estimate is obtained; when the statistical characteristics of the estimated noise are calculated and fused into the Kalman filtering algorithm, the signal obtained by Kalman filtering on the original data is shown in Fig. 8, from which it can be seen that, compared with the wavelet analysis method, the method proposed in this paper has a better filtering effect on the data collected by the magnetic sensor, with less noise and higher SNR.

Positioning experiment: The magnetic field component data of the 16-segment stationary sequences after filtering processing are compared with those of the reference points in the three-axis geomagnetic fingerprint map. Assuming that the noise satisfies the Gaussian distribution, the range of matching points is limited according to three sigma error rate; the absolute error sum of the distance from the matching point to the previous matching point is calculated, from which the point with the minimum absolute error sum is selected as the final matching point and saved in the matching result matrix; after the matching, the coordinates in the matrix are output.

C. Analysis on Positioning Experiment Results

The sensor moves in the region of the geomagnetic fingerprint, which meets the following assumptions: Suppose A, the sensor is periodically stationary at a certain distance(staying at 16 checkpoints for about 10s), which is to facilitate the generation of magnetic fingerprint; Suppose B, the sensor moves along the preset route during the movement, and the three-axis coordinate system of the sensor does not change relative to the ground coordinate system. This assumption simplifies the course judgment process in the positioning process. The sensor moves along a preset route and collects magnetic fingerprints at 16 stationary points, the relative positions of the 16 points are shown in Fig. 9, the theoretical route shows the preset trajectory of the sensor, which can be used as a priori information to calculate the error of the positioning point in the matching route; The processed test data are matched by the SAD algorithm and the location of this point can be roughly determined according to the magnetic field intensity components in three directions at a certain point, and the sensor's motion path can be plotted as shown in Fig. 9. Comparing the coordinate information of the matching positioning point with that of the theoretical positioning point, it is calculated that there are errors between the three matching points and the theoretical points with the position errors as: 0.6m, 0.8485m, and 1.34m. The maximum error of the positioning point in the positioning experiment

is 1.34m. The positioning experiment is carried out in the indoor area as shown in Fig. 5. The triaxial magnetic field distribution is shown in Fig. 6. The magnetic field distribution in the small area is uniform and the difference of magnetic field strength is small. The result error obtained after matching the test sequence is small and the positioning effect is good.

V. Conclusion

An indoor magnetic positioning method with fusion of wavelet analysis and Kalman is proposed in this paper, which utilizes the wavelet analysis method to estimate the multi-source noise components in the three-dimensional magnetic field signal, and filters off and optimizes the single-point magnetic field signal combined with the Kalman filtering algorithm. Under the precondition that the geomagnetic signal is assumed to satisfy the Gaussian distribution, the denoising effectiveness of the wavelet-Kalman fusion filtering method and the wavelet analysis method on noisy signals is simulated and compared in this paper, verifying that this filtering algorithm can effectively improve the signal-to-noise ratio of the magnetic field signal to be matched; 100 reference points within a 5.4m*5.4m indoor area are acquired to plot the geomagnetic fingerprints, the position coordinates of the 16 segments of stationary sequences in the test sequence are matched and located, and the position error between the matching positioning point and the theoretical positioning point is calculated, of which the maximum error of the positioning point in the positioning experiment is 1.34m, which can meet the basic requirements of indoor positioning.

Here are some additional discussions. Firstly, several factors will affect the accuracy of magnetic field positioning, such as magnetic sensor calibration, working time, etc. These are not the focus of this paper, but we will study these factors in the future in order to improve the accuracy of indoor magnetic field positioning methods. Secondly, although our magnetic field fingerprint only reflects the magnetic field distribution in two-dimensional plane, this technology can be applied to the magnetic field distribution in multi-dimensional and three-dimensional space. For example, we can collect the magnetic field information in space by placing multiple magnetic sensors with different heights and establish a three-dimensional magnetic field distribution fingerprint.

Acknowledgment

The authors would like to thank the Shanxi Provincial Key Laboratory of Information Testing and Processing, North University of China, for their strong support for the research on this subject. They would also like to thank Lianbin Wang, Wenbin Bai, Peng Wen, Shichao Zhou, Wei Liu, Jiangang Sun, and other students for their careful help.

References

[1] A. Basiri *et al.*, "Indoor location based services challenges, requirements and usability of current solutions," *Comput. Sci. Rev.*, vol. 24, pp. 1–12, May 2017, doi: 10.1016/j.cosrev.2017.03.002.

[2] C. T. Li, J. C. P. Cheng, and K. Chen, "Top 10 technologies for indoor positioning on construction sites," *Autom. Constr.*, vol. 118, no. 4, Oct. 2020, Art. no. 103309, doi: 10.1016/j.autcon.2020.103309.

[3] A. Poulose and D. S. Han, "Hybrid indoor localization using IMU sensors and smartphone camera," *Sensors*, vol. 19, no. 23, p. 5084, Nov. 2019, doi: 10.3390/s19235084.

[4] Z. An, Q. Lin, L. Yang, and Y. Guo, "Revitalizing ultrasonic positioning systems for ultrasound-incapable smart devices," *IEEE Trans. Mobile Comput.*, vol. 20, no. 5, pp. 2007–2024, May 2021, doi: 10.1109/tmc.2020.2973159.

[5] X. Du, K. Yang, and D. Zhou, "Mapsense: Mitigating inconsistent WiFi signals using signal patterns and pathway map for indoor positioning," *IEEE Internet Things J.*, vol. 5, no. 6, pp. 4652–4662, Dec. 2018, doi: 10.1109/JIOT.2018.2797061.

[6] X. Zhu, J. Yi, J. Cheng, and L. He, "Adapted error map based mobile robot UWB indoor positioning," *IEEE Trans. Instrum. Meas.*, vol. 69, no. 9, pp. 6336–6350, Sep. 2020, doi: 10.1109/TIM.2020.2967114.

[7] W. A. Cahyadi and Y. H. Chung, "Experimental demonstration of indoor uplink near-infrared LED camera communication," *Opt Exp.*, vol. 26, no. 15, pp. 19657–19664, Jul. 2018, doi: 10.1364/OE.26.019657.

[8] C. Yao and W. Hsia, "An indoor positioning system based on the dual-channel passive RFID technology," *IEEE Sensors J.*, vol. 18, no. 11, pp. 4654–4663, Jan. 2018, doi: 10.1109/JSEN.2018.2828044.

[9] Y. Zhuang *et al.*, "A survey of positioning systems using visible LED lights," *IEEE Commun. Surveys Tuts.*, vol. 20, no. 3, pp. 1963–1988, 3rd Quart., 2018, doi: 10.1109/COMST.2018.2806558.

[10] H. Guo, H. Li, J. Xiong, and M. Yu, "Indoor positioning system based on particle swarm optimization algorithm," *Measurement*, vol. 134, pp. 908–913, Feb. 2019, doi: 10.1016/j.measurement.2018.12.038.

[11] N. Yu, X. Zhan, S. Zhao, Y. Wu, and R. Feng, "A precise dead reckoning algorithm based on Bluetooth and multiple sensors," *IEEE Internet Things J.*, vol. 5, no. 1, pp. 336–351, Feb. 2018, doi: 10.1109/JIOT.2017.2784386.

[12] S. Lee, S. Chae, and D. Han, "ILoA: Indoor localization using augmented vector of geomagnetic field," *IEEE Access*, vol. 8, pp. 184242–184255, 2020, doi: 10.1109/ACCESS.2020.3029281.

[13] W. Chen, J. Xu, X. Zhao, Y. Liu, and J. Yang, "Separated sonar localization system for indoor robot navigation," *IEEE Trans. Ind. Electron.*, vol. 68, no. 7, pp. 6042–6052, Jul. 2021, doi: 10.1109/TIE.2020.2994856.

[14] F. J. Gonzalez-Castano, F. Gil-Castineira, D. Rodriguez-Pereira, J. A. Regueiro-Janeiro, S. Garcia-Mendez, and D. Candal-Ventureira, "Self-corrective sensor fusion for drone positioning in indoor facilities," *IEEE Access*, vol. 9, pp. 2415–2427, 2021, doi: 10.1109/ACCESS.2020.3048194.

[15] A. Poulose and D. S. Han, "Hybrid deep learning model based indoor positioning using Wi-Fi RSSI heat maps for autonomous applications," *Electronics*, vol. 10, no. 1, p. 2, Dec. 2020, doi: 10.3390/electronics10010002.

[16] K. Yamashita *et al.*, "Smart hospital infrastructure: Geomagnetic in-hospital medical worker tracking," *J. Amer. Med. Inform. Assoc.*, vol. 28, no. 3, pp. 477–486, Mar. 2021, doi: 10.1093/jamia/ocaa204.

[17] A. Poulose and D. S. Han, "UWB indoor localization using deep learning LSTM networks," *Appl. Sci.*, vol. 10, no. 18, p. 6290, Sep. 2020, doi: 10.3390/app10186290.

[18] G. Wang, X. Wang, J. Nie, and L. Lin, "Magnetic-based indoor localization using smartphone via a fusion algorithm," *IEEE Sensors J.*, vol. 19, no. 15, pp. 6477–6485, Aug. 1, 2019, doi: 10.1109/JSEN.2019.2909195.

[19] I. Ashraf, M. Kang, S. Hur, and Y. Park, "MINLOC:Magnetic field patterns-based indoor localization using convolutional neural networks," *IEEE Access*, vol. 8, pp. 66213–66227, 2020, doi: 10.1109/ACCESS.2020.2985384.

[20] Z. Liu, L. Zhang, Q. Liu, Y. Yin, L. Cheng, and R. Zimmermann, "Fusion of magnetic and visual sensors for indoor localization: Infrastructure-free and more effective," *IEEE Trans. Multimedia*, vol. 19, no. 4, pp. 874–888, Apr. 2017, doi: 10.1109/TMM.2016.2636750.

[21] X. Qi *et al.*, "Bioinspired in-grid navigation and positioning based on an artificially established magnetic gradient," *IEEE Trans. Veh. Technol.*, vol. 67, no. 11, pp. 10583–10589, Nov. 2018, doi: 10.1109/TVT.2018.2866428.

[22] Y. Shu, C. Bo, G. Shen, C. Zhao, L. Li, and F. Zhao, "Magicol: Indoor localization using pervasive magnetic field and opportunistic WiFi sensing," *IEEE J. Sel. Areas Commun.*, vol. 33, no. 7, pp. 1443–1457, Jul. 2015, doi: 10.1109/JSAC.2015.2430274.

[23] K.-M. Lee, M. Li, and C.-Y. Lin, "Magnetic tensor sensor and way-finding method based on geomagnetic field effects with applications for visually impaired users," *IEEE/ASME Trans. Mechatronics*, vol. 21, no. 6, pp. 2694–2704, Dec. 2016, doi: 10.1109/TMECH.2016.2582850.

[24] B. Kim and S.-H. Kong, "A novel indoor positioning technique using magnetic fingerprint difference," *IEEE Trans. Instrum. Meas.*, vol. 65, no. 9, pp. 2035–2045, Sep. 2016, doi: 10.1109/TIM.2016.2566759.
[25] B. Bhattarai, R. K. Yadav, H.-S. Gang, and J.-Y. Pyun, "Geomagnetic field based indoor landmark classification using deep learning," *IEEE Access*, vol. 7, pp. 33943–33956, 2019, doi: 10.1109/ACCESS.2019.2902573.
[26] G. Liu, B. Yu, L. Huang, L. Shi, X. Gao, and L. He, "Human-interactive mapping method for indoor magnetic based on low-cost MARG sensors," *IEEE Trans. Instrum. Meas.*, vol. 70, 2021, Art. no. 9505510, doi: 10.1109/tim.2021.3052026.
[27] L.-F. Shi, R. He, and B.-L. Feng, "Indoor localization scheme using magnetic map for smartphones," *Wireless Pers. Commun.*, Aug. 31, 2021, doi: 10.1007/s11277-021-08951-w.
[28] Z. Zhang, X. Niu, H. Tang, Q. Chen, and T. Zhang, "GNSS/INS/ODO/wheel angle integrated navigation algorithm for an all-wheel steering robot," *Meas. Sci. Technol.*, vol. 32, no. 11, Nov. 2021, Art. no. 115122, doi: 10.1088/1361-6501/ac17fb.
[29] A. Poulose, O. S. Eyobu, and D. S. Han, "An indoor position-estimation algorithm using smartphone IMU sensor data," *IEEE Access*, vol. 7, pp. 11165–11177, 2019, doi: 10.1109/access.2019.2891942.
[30] J. Grottke and J. Blankenbach, "Evolutionary optimization strategy for indoor position estimation using smartphones," *Electronics*, vol. 10, no. 5, p. 618, Mar. 2021, doi: 10.3390/electronics10050618.
[31] H. Huang, W. Li, D. A. Luo, D. W. Qiu, and Y. Gao, "An improved particle filter algorithm for geomagnetic indoor positioning," *J. Sensors*, vol. 2018, pp. 1–9, Mar. 2018, doi: 10.1155/2018/5989678.
[32] A. Poulose, J. Kim, and D. S. Han, "A sensor fusion framework for indoor localization using smartphone sensors and Wi-Fi RSSI measurements," *Appl. Sci.*, vol. 9, no. 20, p. 4379, Oct. 2019, doi: 10.3390/app9204379.
[33] Y. Ma, Z. Dou, Q. Jiang, and Z. Hou, "Basmag: An optimized HMM-based localization system using backward sequences matching algorithm exploiting geomagnetic information," *IEEE Sensors J.*, vol. 16, no. 20, pp. 7472–7482, Oct. 2016, doi: 10.1109/JSEN.2016.2600099.
[34] X. Wang, C. Zhang, F. Liu, and X. Xu, "Exponentially weighted particle filter for simultaneous localization and mapping based on magnetic field measurements," *IEEE Trans. Instrum. Meas.*, vol. 66, no. 7, pp. 1658–1667, Jul. 2017, doi: 10.1109/TIM.2017.2664538.
[35] C. Chou, H. Li, and D. Song, "Encoder-camera-ground penetrating radar sensor fusion: Bimodal calibration and subsurface mapping," *IEEE Trans. Robot.*, vol. 37, no. 1, pp. 67–81, Feb. 2021, doi: 10.1109/tro.2020.3010640.
[36] Z. Xian and H. Yang, "An early warning model for the stuck-in medical drilling process based on the artificial fish swarm algorithm and SVM," *Distrib. Parallel Databases*, Jul. 7, 2021, doi: 10.1007/S10619-021-07344-Z.
[37] S.-Y. Lee, J.-Y. Sim, C.-S. Kim, and S.-U. Lee, "Correspondence matching of multi-view video sequences using mutual information based similarity measure," *IEEE Trans. Multimedia*, vol. 15, no. 8, pp. 1719–1731, Dec. 2013, doi: 10.1109/TMM.2013.2271747.

Kai Li (Member, IEEE) received the Ph.D. degree in signal and information processing from the North University of China, China, in 2017.

He is currently an Associate Professor of Signal and Information Processing. Since 2010, he has been involved in magnetic sensor design on integrated transceivers. He holds five patents. His current research interests include electromagnetics and sensor.

Qingqing Gong was born in Yichang, Hubei, in 1996. She received the bachelor's degree in information confrontation from the School of Information and Communication Engineering, North University of China, in 2018, where she is currently pursuing the master's degree in electronics and communication engineering.

Her research interests include geomagnetic field positioning technology and signal processing methods.

Yajun Ren was born in Changzhi, Shanxi, China, in 1996. She received the bachelor's degree in information confrontation from the North University of China in 2018, where she is currently pursuing the master's degree in information and communication engineering.

Her research interest includes simulation of array electromagnetic excitation sources.

Yuan Li received the Ph.D. degree in weapon science and technology from the North University of China, China, in 2014.

She is currently an Associate Professor and a Master Supervisor in signal and information processing. Her main research interests include signal and information processing, optical device, and sensor.

Yan Han received the Ph.D. degree from the Beijing Institute of Technology, China, in 1998.

He is currently a Professor of Signal and Information Processing. Since 1998, he has been a Supervisor and the Director of the Research Center in computer aided electrical engineering. His main research interests include signal and information processing destructive detection and sensor.

Cunsuo Pang received the Ph.D. degree in electronics engineering from the School of Information and Electronics, Beijing Institute of Technology, China, in 2014. He is currently a Lecturer with the School of Information and Communication Engineering, North University of China. His research interests include radar signal processing and time-frequency analyses.

Huihua Kong received the B.S. degree in statistics and probability from Shanxi University in 2001 and the M.S. degree in signal and information processing and the Ph.D. degree in information processing and reconstruction from the North University of China, China, in 2011. Since 2012, she has been an Associate Professor with the School of Science, North University of China. Her research interests include computed tomography image reconstruction and signal and image processing.